Three-dimensional metrology of microturning tool edge radii

Mayra Yucely Beb[a], Yanis Tadjouddine[b], Alexandre Boucheny[b], Olivier Lehmann[a], Jean-Yves Rauch[a], Sounkalo Dembélé[a], Nadine Piat[b] and Sébastien Thibaud[b,*]

[a] *Université de Franche-Comté, CNRS, FEMTO-ST Institute, AS2M Departement, 26 rue de l'Epitaphe, Besancon, France*
[b] *SupMicroTech ENSMM, CNRS, FEMTO-ST Institute, Department of Applied Mechanics, 24 rue de l'Epitaphe, Besancon, France*

ARTICLE INFO

Keywords:
Tool edge radius measurement
3D reconstruction
Robust 3D curve fitting
Robust optimization
Photon Microscope
Scanning Electron Microscope
Micro turning

ABSTRACT

The cutting edge radius is a significant parameter of a micromachining tool. When it is not sufficiently sharp, ploughing, which affects the whole machining process and workpiece quality, will occur. It is then essential to be able to estimate the value of the cutting edge radius accurately. In this paper, a three-dimensional strategy that can be used to measure the microturning tool edge radii is presented. The strategy is based on robust cylinder fitting that is applied to a 3D point cloud of the tool. It is implemented in C++ with Open Computer Vision and Point Cloud Library. It was validated using a virtual point cloud, resulting in errors of 0.42% and 1.11% without noise and with noise, respectively. Additionally, uncertainties of 0.045 µm and 0.082 µm were obtained. It was successfully applied to six microturning inserts: three unused tools and three used tools. The point clouds were obtained with two different 3D surface reconstruction techniques, focus variation with a photon microscope and a multi-view stereo with a scanning electron microscope. The obtained results were more coherent, i.e., they were less dispersed; for example, in non-used tools, the range was [3.11 µm-3.90 µm] and for the conventional circle fitting the range was [2.62 µm-4.38 µm]. The traditional method is indirect: the 3D point cloud is sliced into 2D point clouds (profiles) fitted with circles. This 3D-2D process might result in errors. The proposed method is a direct 3D approach with no slicing step.

1. Introduction

1.1. Context

Micromachining is defined as a cutting process at a submillimetre scale [1], [2]. In the cases of milling and turning, it is a downscaling of classical processes. Nevertheless, this reduction in scale is not hypothetically identical for all parameters, particularly for the tool's microgeometries. Then, the assumption of a perfectly sharp cutting edge of the tool is no longer valid in micromachining, and it is then considered as having a radius that is called the sharp cutting edge radius [3].

The cutting edge is influenced by many parameters, including the size of the tool carbide grain, the thickness of the coating and the manufacturing process of the tool [4], [5], [6], [7]. Therefore, it is rarely considered to be less than 1 µm and is not uniform along the tool edge. Compared to the thickness of the undeformed chip, it is sometimes in the same order of magnitude. This suggests that the cutting process is more complex with, for example, an apparent cutting angle different from the nominal angle or even strongly negative during machining. More particularly, when the cutting edge radius is not sharp enough, no chip is formed during cutting, i.e., a ploughing phenomenon occurs, as highlighted by Vogler et al. [8], Lee and Dornfeld [9], Jun et al. [10], Xu et al. [7], Celaya et al. [11] and Woon et al. [12]. It strongly influences cutting forces, energy, temperature, residual stress in the workpiece, and the quality of the workpiece after machining. To model the ploughing phenomenon, it is necessary to be able to determine the cutting-edge radius with accuracy.

1.2. State-of-the-Art Methods

Many scholars have already investigated the problem of cutting-edge radius measurement, with many commercial solutions available. The problem is challenging because of the tool's small size (which makes it very difficult to

*Corresponding author: Department of Applied Mechanics, 24 rue de l'épitaphe, F-25000 Besançon, France
Phone: (+33) 3 81 66 66 11 - Fax: (+33) 3 81 66 66 01
sebastien.thibaud@ens2m.fr (S. Thibaud)
ORCID(s):

manipulate) and the small radius (which is approximately a tenth of a micrometer, which requires a high-resolution measurement system). The solutions that include the acquisition of data and their processing are classified as destructive and non-destructive, depending on whether or not data acquisition involves tool edge destruction. In both cases, it is a matter of circle fitting until now. The most common criteria for fitting circles are the Gaussian condition or least square circle, minimum zone circle, minimum circumscribed circle, and maximum inscribed circle Wyen et al. [13].

Akbari et al. [5] and Wyen et al. [13] provided insights into the problem. They stated that the conventional method, which is standard, is based on least squares circle fitting. For 2D data, i.e., profiles, typically obtained from a tactile profilometer, straight lines that fit the points of both faces of the edge (rake and flank) are retrieved, and the circle that best fits the curved part of the profile is computed [13]. The average radius of a set of best-fitted circles defines the cutting-edge radius. For 3D data, i.e., 3D point clouds, a cross-section perpendicular to the cutting edge is first defined, leading to a cross-section profile. Then, the above procedure is used.

Akbari et al. [5] compared the results for five measurement instruments implementing circle fitting:

- A profilometer (Form Talysurf Series 2 in association with Ultra software, from Taylor Hobson, UK);
- A confocal microscope with associated software (Leica Map DCM 3D, Germany);
- A focus-variation microscope with associated software (InfiniteFocus Real3D from Alicona Imaging, Austria);
- A scanning electron microscope (SEM) in association with MeX software, from Alicona Imaging, for 3D reconstruction;
- An atomic force microscope (AFM) and associated software (MFP-3D from Asylum Research, CA, USA) were used.

For a set of single crystalline synthetic diamonds, the measurement uncertainties increased progressively from AFM, SEM, confocal microscopy, and tactile profilometry to focus-variation microscopy.

Furthermore, for single-point diamond tools, some researchers used an AFM [14] (SPA 500 from Seiko, Japan), [15], [16], [17] (Innova from Bruker, USA), and [18], a scanning probe microscope (SPM) [19] or an SEM [20].

For a two-flute carbide micro-ball end mill, Baburaj et al. [21] used a laser microscope (LEXTOLS4000 3D from Olympus) as a profilometer and a stereo-microscope (STEMI 2000-CS from Zeiss, Germany) for 3D modelling. Axio Vision software from Zeiss was used for data processing in both cases. After comparison with a destructive approach using SEM (the tool was sectioned using a diamond cutting technique, and a 2D image of the edge profile was fitted with a circle), the authors concluded the reliability of the non-destructive solution.

Celaya et al. [11] explored the influence of various geometry parameters, namely, the clearance angle, rake angle, and cutting edge radius, on the tool life and specific aspects, such as the tool wear depth, during milling. They found that the cutting-edge radius has the most significant impact on the tool wear depth. The cutting edge radius was obtained with a DF70 OTEC drag finishing machine and measured with an Alicona Infinite Focus microscope.

For cutting tool inserts, Lim and Ratnam [22] proposed a solution consisting of acquiring 2D images of the tool with a CCD (charged-coupled device) flatbed scanner (CanoScan 5600F, Japan) and extracting the edge profiles from the obtained images. The obtained results were similar to those of the focus-variation approach (Alicona InfiniteFocus microscope).

The core of the conventional tool edge radius measurement solution is 2D metrology. Even if the input data are a 3D point cloud, the latter can be sliced into 2D point clouds, i.e., profiles, that are fitted with circles [23], [17]. This slicing could be a source of inaccuracy, especially when profiles need to be perpendicular to the tool edge. This issue, combined with the wide use of 3D imaging systems (3D confocal microscopy, 3D focus-variation microscopy, 3D SEM, 3D AFM), raises the requirement of 3D metrology for tool edge radius measurement. Recently, the company Novacam proposed this kind of solution; unfortunately, this solution is not documented [24].

1.3. Contribution

In the proposed technique, an accurate and reliable 3D metrology solution based on robust optimization is developed for tool edge radius measurement. The user selects a 3D region of interest (ROI) from only two 3D points. This global ROI is progressively scanned from a few initial 3D points to all points, and each selected 3D point set is best fitted with a cylinder. A curve of the fitted cylinder radii with regards to the scan steps is obtained. In this curve, the intersection with the y-axis determines the edge radius. The method is direct, with the 3D to 2D slicing process being avoided since it could result in errors.

[Fig. 1 about here.]

The method is implemented in C++ using PCL (Point Cloud Library) for 3D point cloud processing and Robest's algorithm for line fitting estimation [25], more particularly, in both cases, robust least squares implementations [26]. A virtual edge point cloud was considered as an initial step for the theoretical validation of the method. For the final validation, six microturning tools, typically used for finishing and shape operations, are considered. For each case, two techniques were employed to obtain the point clouds:

- Focus Variation with Photon Microscopy: Focus variation was performed using the μCMM machine manufactured by Bruker Alicona with a minimum resolution of 20nm [27]. The measurement setup involved applying a 50X magnification, a rotation angle of 7.755°, and an inclination angle of -0.902°.
- Multiview stereo with Scanning Electron Microscopy (SEM): The acquisition of SEM images involved capturing five images, each obtained with a 1° degree difference in inclination, and applying 700X magnification. Instead of using commercial software, Pollen3D, which is an internal 3D reconstruction application for SEM, was employed [28], [29], [30], [31]. Pollen3D is based on the OpenCV (Open Computer Vision library) and NLOpt (Non-Linear Optimization) library.

The effectiveness of the cylinder fitting method was demonstrated by applying it to a set of point clouds acquired through these two techniques. The results were then compared with those obtained from EdgeMaster software from Alicona, the edge radius accuracy is based on ISO 10360-8 and VDI 2617, the uncertainty is 1.5um [27], which uses the conventional circle fitting technique.

2. Conventional edge radius measurement

Classically, the tool edge radius measurement is defined according to the following procedure and in relation to Fig. 2 [5]:

- Step 1: Local scanning of the cutting area to obtain a 3D point cloud of that area;
- Step 2: Definition of the section plane (cross-section or profile, i.e., set of 2D points) along the cutting edge (the normal to the section plane is theoretically equal to the local tangent vector of the cutting edge);
- Step 3: Determination of the points belonging to the section plane;
- Step 4: Determination of the intersection lines between the section plane and the rake and clearance planes by a best-fit method and a new point concerning the intersection point of both lines;
- Step 5: Determination by a least square approximation method of the circle tangent to the intersection lines and the new point;
- Step 6: Application of the above steps to several cross-section planes along the cutting edge;
- Step 7: The mean radius of the obtained fitting circles is then considered to be the value of the edge radius.

[Fig. 2 about here.]

Realistically, this method is not reliable enough to be considered. Indeed, it is based on the accuracy of the second step, the definition of the cross-section plane, which corresponds to the slicing of the 3D point cloud into 2D point clouds. Moreover, it is quite difficult to perfectly determine any section plane perpendicular to the cutting edge. According to Fig. 2, the two intersection profiles are similar, but only one section plane is correct in the definition of the cutting edge radius. In the case of the second section plane, the local edge radius will be overestimated and leads to an incorrect approximation. Consequently, the other steps are constrained by the cross-section definition. Therefore, a new method is required to prevent this issue.

[Fig. 3 about here.]

[Fig. 4 about here.]

In the following section, the lack of perpendicularity of the cross-section plane with the cutting edge will be quantified. Assuming the latter is a cylinder (with a radius of 1 μm), a circular regression is performed to fit the obtained geometric shape resulting from the intersection of a plane, having an angle of inclination to the axis of this cylinder. When the plane is perfectly perpendicular to the cylinder (the angle of inclination is 0°), the intersection shape is a perfect circle (Fig. 3); otherwise, it is an ellipse (Fig. 4). The least square approximation method was used for the fitting circle; at 0 ° of inclination, the result radius was 1.04 μm, and at 30 °, it measured 1.12 μm, as depicted in Figs. 3 and 4.

[Fig. 5 about here.]

It was observed (Fig. 5) that the estimated radius closely aligns with the target value at an inclination angle of 0° and gradually increases up to 14% at a maximum inclination angle of 45°.Based on these findings, the influence of the perpendicularity between the cross-section plane and the edge radius might not be deemed negligible.

3. Three-dimensional edge radius measurement

In the present study, a novel approach for measuring the edge radius is introduced. This method does not have the limitations of the traditional method. The developed methodology is implemented by using the open-source libraries OpenCV (version 4.5.4) and PCL (version 1.13.0). The core functionality of the application relies on robust least squares optimization techniques. Specifically, the PCL implementation of the least median of squares (LMedS) is employed to obtain the parametric model for plane and cylinder fitting of point cloud data. Additionally, robust line fitting using LMedS is employed.

In the subsequent sections, visual representations of the various steps involved in the application's workflow are provided.

3.1. Selection of the global region of interest

Two points P_1 and P_2 are interactively selected on the cutting region of the tool on the point cloud. These two points describe a segment used as the cylinder's axis with a specified radius. All the points inside this cylinder make the 3D region of interest (as shown in Fig. 6). The two points must be carefully selected because they must be in the region of interest. A line that must pass through the region of interest is displayed. If this does not happen, the points must be reselected.

[Fig. 6 about here.]

3.2. Fitting local regions of interest with cylinders

From the initial global ROI, one hundred local ROIs with increasing radius sizes are selected around the line defined by the points P_1 and P_2. Then, the points inside every local ROI of radius r_{ROI} are fitted with cylinders using the PCL sample consensus library with the LMedS algorithm. For each value r_t of the cylinder, the estimated radius (stated measured or experimental radius) is stored for analysis. The parameters of the application are the threshold of the fitting algorithm (set to 0.1 µm in this paper), the minimum and maximum radii (set to 1µm and 100µm, respectively), and the scan step (here 0.1µm). These parameters must be adapted to the desired resolution of the measurement.

3.3. Estimation of radius

The resulting set of the cylinder radii (r_t) can be represented with the ROI radii (r_{ROI}). The theoretical foundation of the method states that during the estimation of the cutting edge radius, a region of instability (non-linear zone) is expected to be observed at the initial and final parts of the obtained curve (Fig. 7). Conversely, a region of stability, such as an approximately linear area, might be found between the initial and final parts. Indeed, for a small or large ROI consistently centred around the cutting edge, it is evident that the shape of the cutting tool significantly deviates from that of a cylinder. As a result, the estimation process becomes increasingly unstable, leading to unreliable results. The point cloud data of a stable region represent a portion of a cylinder. This partial cylindrical shape enables us to successfully estimate the radius, as it exhibits a relatively stable and consistent pattern.

[Fig. 7 about here.]

The cutting edge radius of the tool is determined through the intersection of two lines, as depicted in Fig. 7. One line corresponds to the estimation obtained on the stable region of the data using the Robest algorithm [25], while the other line has the equation $x = 0$ (representing the y-axis). Although the line estimated by the Robest algorithm might not always be perfectly straight due to the influence of the acquired data, the intersection is calculated with the first point in the data. In essence, by knowing the equation of the line estimated by Robest and the x-coordinate of the first data point, the cutting radius can be directly determined by calculating the corresponding y-coordinate.

4. Application to a virtual tool

To assess the effectiveness of the edge radius measurement method (cylinder fitting), a virtual tool was employed for evaluation purposes. The virtual tool was assigned an arbitrary cutting-edge radius of $r_t = 8.05\ \mu m$. Subsequently, measurements were conducted on this virtual tool in two scenarios: one without any added noise and another with the introduction of normal noise (Fig. 8).

[Fig. 8 about here.]

The measuring experiment was repeated ten times for each scenario to ensure reliability and assess the method's robustness. In each iteration, different points ($P1$ and $P2$) were chosen to capture variations and potential sources of error (Fig. 9).

[Fig. 9 about here.]

[Table 1 about here.]

Application to the perfect virtual cutting tool yielded highly satisfactory results. The average r_t obtained from these simulations was 8.052 µm and the maximum error obtained was 1.2% (Table 1). Fig. 10(a) presents one of the results.

In addition, experiments were conducted on the tool on which normal noise was added. Even if this type of noise might significantly differ from the usual noises on real tools, it is a good indicator of how the method responds to perturbations. Fig. 8(b) shows the obtained data for 300 steps ($r_{ROI} = [1 : 0.1 : 30]$), with a $[\mu = 0\ \mu m; 3\sigma = 0.1\ \mu m]$ noise amplitude normally distributed along the three directions. According to our method, the average measured r_t in the virtual tool with noise was 8.11 µm, and the maximum error obtained was 2.23% (Table 1). Fig. 10(b) presents one of the test results.

[Fig. 10 about here.]

Fig. 11 displays the full results obtained with the virtual cutting tool.

The obtained results show a commendable level of accuracy when applied to point clouds that were perfectly formed. Even in the presence of substantial noise, the method performed adequately, although the accuracy was somewhat compromised under such conditions. These results, which align with the theoretical expectations, confirm the method's effectiveness. This indicates high precision and consistency in the edge radius measurement method.

[Fig. 11 about here.]

5. Application to real tools

5.1. Procedure

The edge radius measurement method is applied to six micro-precision Swiss turning tools 050RK18BI90 from BIMU SA [32], three non-use and three used (Fig. 12). As previously mentioned, two techniques were employed for the 3D surface reconstruction of the cutting tools. These techniques include:

- Focus variation with photon microscopy: A µCMM machine from Bruker Alicona was used. This method entailed capturing the surface profile of the cutting tools using a 50X magnification, along with specific rotation and inclination angles. Fig. 13(a) represents one of the dataset's images used for the 3D surface reconstruction process with the focus-variation technique;

- Multiview stereo with SEM: This technique involved capturing a series of five images with an Auriga SEM (Auriga from Zeiss, Germany) with varying degrees of inclination and applying a high magnification factor (700X) and pixel size of 162.7nm. The pollen 3D application developed in our lab, described in appendix A and available on git [29], was used to perform 3D reconstruction of the tools. Fig. 13(b) represents one of the dataset's images used for the 3D surface reconstruction.

[Fig. 12 about here.]

[Fig. 13 about here.]

A comparison was made between the number of points obtained in the 3D reconstruction of each sample using the two different techniques. It was observed that the multi-view stereo with SEM yielded double the number of points compared to the focus variation with photon microscopy. This can be attributed to the SEM's ability to capture more detailed characteristics and use a high magnification factor during data acquisition. Fig. 14 visually compares the number of points in the 3D reconstructions based on the respective techniques.

[Fig. 14 about here.]

Three different results were obtained and compared. The first result was obtained using the proposed, precise cylinder fitting method applied to the point clouds acquired through the focus-variation technique. The second result was obtained using the same method but applied to the point clouds generated using the multi-view stereo technique. The third result involved using the conventional circle fitting technique on the point cloud acquired through the focus-variation technique using the commercial software provided by Alicona (Tool edge measurements).

5.2. Results

Fig. 15 shows measured radii values according to the local ROIs' sizes using the point clouds from the focus-variation method and the multi-view stereo for two tools (Unused-3, Used-3). As explained previously, multiple local ROIs are selected and centred around the cutting edge, with a progressively increasing size. The results are coherent: 3.48 µm and 3.43 µm for Unused-3 from focus variation and multi view stereo, respectively; and 5.01 µm and 5.06 µm for Used-3 from focus variation and multi-view stereo, respectively.

Furthermore, the conventional circle fitting technique was also employed for comparison. Fig. 16 illustrates the results obtained with the same tools (Unused-3 and Used-3) from point clouds generated through focus-variation/photo microscopy. The obtained edge radii were 3.629 µm and 4.917 µm for Unused-3 and Used-3, respectively. These values are favorable and of the same order of magnitude as those obtained previously. At this stage, both measurement methods cannot be compared.

Fig. 17 compares the results obtained from the analysis of six cutting tools: three were not used (Non Used-1, Non Used-2, and Non Used-3), whereas three were used (Used-1, Used-2, Used-3). For each tool, the comparison involved applying three scenarios: circle fitting with focus-variation/photon microscopy, cylinder fitting with focus-variation/photon microscopy, and cylinder fitting with multi-view stereo/SEM. For unused tools, the edge radius ranged from 3.11 µm and 3.90 µm with the developed cylinder fitting method, whereas it ranged from 2.62 µm and 4.38 µm with the conventional method. For the tools used, the edge radius ranged from 3.86 µm and 5.91 µm with the developed cylinder fitting method, whereas it ranged from 3.19 µm and 19.87 µm with the conventional method. In all non-used cases, the results of cylinder fitting are in the same range as those of circle fitting. Moreover, the edge radii are of the same order of magnitude with a limited dispersion.

[Fig. 15 about here.]

[Fig. 16 about here.]

[Fig. 17 about here.]

6. Conclusion

In this paper, a method for measuring the cutting-edge radius of microturning tools from 3D point clouds is proposed. It is a direct method that estimates the radius of the cylinder best fitting the tool 3D point cloud. Therefore, the potential errors that might occur from slicing the 3D point cloud into 2D profiles can be avoided.

The method was implemented in C++ with open-source libraries: Open Computer Vision (OpenCV) library, Point Cloud Library (PCL), and Robust estimation library (Robest). The 3D point clouds obtained with the focus-variation method with photon microscopy images of the μCMM machine from Bruker-Alicona and multi-view stereo with scanning electron microscopy images and Pollen3D from our lab were used.

The method was validated theoretically with a cylinder as a virtual tool and experimentally with six tools: three unused tools and three used tools. In all cases, the results of the developed cylinder fitting method were more coherent, i.e., they are less dispersed, for example, non-used tools, the range is [3.11μm-3.90μm] than the conventional circle fitting (EdgeMaster from Bruker-Alicona), the range is [2.62μm-4.38μm]. Moreover, the edge radii were of the same order of magnitude with a limited dispersion.

This comparative evaluation allowed for an assessment of the performance of the cylinder fitting method compared to the conventional circle fitting method, providing evidence of the method's relevance and suitability for the given application.

The main limitation of this method is the geometry of the tool edge to measure: it should be close to a cylinder. An additional limitation lies in the manual selection of the area of interest, specifically in the selection of points (P1 and P2). This manual process has to be done very carefully.

There are various applications where this method can be applied. Knowing the cutting radius of a tool is crucial in the cutting process. For instance, when the cutting edge radius is not sharp enough, no chip is formed during cutting, leading to a ploughing phenomenon. Measuring this radius accurately beforehand can significantly improve the final results in cutting processes. However, this is just one example of its potential utility.

In the future, the method will be extended to address more advanced geometries, such as the micro-milling tool (helical shape).

Acknowledgements

The Equipex ROBOTEX project (contract ANR-10-EQPX-44-01) supported the experiments. The authors would like to thank the platform MIFHySTO facility for access to the equipment.

A. Pollen 3D, a 3D reconstruction application of the type multi-view stereo based on autocalibration

Even if there exist many applications for reconstructing 3D point clouds from the images of scanning electron microscope (MeX from Alicona, Austria; Mountains from Digital Surf, France; 3DSEM from Zeiss, Germany; etc.), we chose to develop our application in C++ with open-source libraries OpenCV [33], PCL [26] and NLOpt [34]: Pollen 3D. Indeed, current applications that are geometry-based (only 3DSEM that uses 4-quadrant detectors is photometry based) use the values of sample rotation taken directly from the SEM interface (Kratochvil et al. [35], Jähnisch and Fatikow [36], Baghaie et al. [37] MeX, Mountains, etc.). However, our experience in SEM showed that the accuracy of these values is no longer guaranteed because of errors in the sample positioning concerning SEM eucentric points. To overcome this problem, Pollen 3D is used to accurately compute the sample rotations, along with an SEM, from an autocalibration approach [29], [38], and they are then used to compute the 3D point cloud.

Before starting the application, at least three images must be acquired by rotating the sample approximately 3-10 degrees with an SEM platform or additional robot manipulator.

The first step of the application is autocalibration, i.e., automatic and accurate estimation of rotations (usually motions), along with the model.

The next step involves rectifying image pairs, i.e., making them coplanar and easy to match. Next, dense matching link points in pairs and disparity maps are computed.

Finally, a direct triangulation is implemented as described in Xie [39] and Baghaie et al. [37] to obtain a 3D point cloud that we filter out. Pollen 3D is available on git: Kudryavtsev et al. [29].

References

[1] Masuzawa, T. (2000). State of the Art of Micromachining. *CIRP Annals*, 49(2), 473–488. 0007-8506. 10.1016/S0007-8506(07)63451-9. https://www.sciencedirect.com/science/article/pii/S0007850607634519.

[2] Dornfeld, D., Min, S., Takeuchi, Y. (2006). Recent Advances in Mechanical Micromachining. *CIRP Annals*, 55(2), 745–768. 0007-8506. 10.1016/j.cirp.2006.10.006. https://www.sciencedirect.com/science/article/pii/S1660277306000077.

[3] Bissacco G, Hansen HN, De Chiffre L. Micromilling of hardened tool steel for mould making applications. J Mater Process Technol 2005;167(2):201–207. URL: https://www.sciencedirect.com/science/article/pii/S0924013605006187. doi:10.1016/j.jmatprotec.2005.05.029

[4] Denkena B, Biermann D. Cutting edge geometries. CIRP Ann 2014;63(2):631–653. URL: https://www.sciencedirect.com/science/article/pii/S0007850614001917. doi:10.1016/j.cirp.2014.05.009

[5] Akbari M, Knapp W, Wegener K. Comparison of transparent objects metrology through diamond cutting edge radii measurements. CIRP J Manuf Sci Technol 2016;13:72–84. URL: https://www.sciencedirect.com/science/article/pii/S1755581715000747. doi:10.1016/j.cirpj.2015.12.001

[6] Bernard SE, Selvaganesh R, Khoshick G, Samuel Raj D. A novel contact area based analysis to study the thermo-mechanical effect of cutting edge radius using numerical and multi-sensor experimental investigation in turning. J Mater Process Technol 2021;293:117085. URL: https://www.sciencedirect.com/science/article/pii/S0924013621000455. doi:10.1016/j.jmatprotec.2021.117085

[7] Xu F, Wang J, Fang F, Zhang X. A study on the tool edge geometry effect on nano-cutting. Int J Adv Manuf Technol 2017;91(5):2787–2797. URL: https://doi.org/10.1007/s00170-016-9922-4. doi:10.1007/s00170-016-9922-4

[8] Vogler MP, DeVor RE, Kapoor SG. On the modeling and analysis of machining performance in micro-endmilling, Part I: Surface generation. J Manuf Sci Eng 2005;126(4):685–694. URL: https://doi.org/10.1115/1.1813470. doi:10.1115/1.1813470

[9] Lee K, Dornfeld DA. Micro-burr formation and minimization through process control. Precis Eng 2005;29(2):246–252. URL: https://www.sciencedirect.com/science/article/pii/S0141635904001345. doi:10.1016/j.precisioneng.2004.09.002

[10] Jun MBG, DeVor RE, Kapoor SG. Investigation of the dynamics of microend milling–Part II: Model validation and interpretation. J Manuf Sci Eng 2006;128(4):901–912. URL: https://doi.org/10.1115/1.2335854. doi:10.1115/1.2335854

[11] Celaya A, Pereira O, González H, Gómez-Escudero G, Fernández-Lucio P, Fernández-Valdivielso A, et al. Influence of cutting edge radius on tool life in milling inconel 718. AIP Conf Proc 2019;2113(1):080019. URL: https://doi.org/10.1063/1.5112627. doi:10.1063/1.5112627

[12] Woon KS, Rahman M, Neo KS, Liu K. The effect of tool edge radius on the contact phenomenon of tool-based micromachining. Int J Mach Tools Manuf 2008;48(12):1395–1407. URL: https://www.sciencedirect.com/science/article/pii/S0890695508000850. doi:10.1016/j.ijmachtools.2008.05.001

[13] Wyen CF, Knapp W, Wegener K. A new method for the characterisation of rounded cutting edges. Int J Adv Manuf Technol 2012;59(9):899–914. URL: https://doi.org/10.1007/s00170-011-3555-4. doi:10.1007/s00170-011-3555-4

[14] Li XP, Rahman M, Liu K, Neo KS, Chan CC. Nano-precision measurement of diamond tool edge radius for wafer fabrication. In: Scopus. 2003,URL: https://scholarbank.nus.edu.sg/handle/10635/73672; accepted: 2014-06-19T05:37:58Z ISSN: 0924-0136

[15] Zhang K, Cai Y, Shimizu Y, Matsukuma H, Gao W. High-precision cutting edge radius measurement of single point diamond tools using an atomic force microscope and a reverse cutting edge artifact. Appl Sci 2020;10(14):4799. URL: https://www.mdpi.com/2076-3417/10/14/4799. doi:10.3390/app10144799; number: 14 Publisher: Multidisciplinary Digital Publishing Institute

[16] Shimizu Y, Asai T, Gao W, Shimizu Y, Asai T, Gao W. Evaluation of Nanometer Cutting Tool Edge for Nanofabrication. London: IntechOpen; 2011. ISBN 978-953-307-912-7. URL: https://www.intechopen.com/state.item.id. doi:10.5772/28581; publication Title: Nanofabrication

[17] Chen YL, Cai Y, Xu M, Shimizu Y, Ito S, Gao W. An edge reversal method for precision measurement of cutting edge radius of single point diamond tools. Precis Eng 2017;50:380–387. URL: https://www.sciencedirect.com/science/article/pii/S0141635917303392.

doi:10.1016/j.precisioneng.2017.06.012

[18] Gao W, Motoki T, Kiyono S. Nanometer edge profile measurement of diamond cutting tools by atomic force microscope with optical alignment sensor. Precis Eng 2006;30(4):396–405. URL: https://www.sciencedirect.com/science/article/pii/S0141635906000043. doi:10.1016/j.precisioneng.2005.11.008

[19] Liu X, Zhou T, Pang S, Xie J, Wang X. Burr formation mechanism of ultraprecision cutting for microgrooves on nickel phosphide in consideration of the diamond tool edge radius. Int J Adv Manuf Technol 2018;94(9):3929–3935. URL: https://doi.org/10.1007/s00170-017-1079-2. doi:10.1007/s00170-017-1079-2

[20] Asai S, Taguchi Y, Horio K, Kasai T, Kobayashi A. Measuring the very small cutting-edge radius for a diamond tool using a new kind of SEM having two detectors. CIRP Ann 1990;39(1):85–88. URL: https://www.sciencedirect.com/science/article/pii/S0007850607610087. doi:10.1016/S0007-8506(07)61008-7

[21] Baburaj M, Ghosh A, Shunmugam MS. Study of micro ball end mill geometry and measurement of cutting edge radius. Precis Eng 2017;48:9–17. URL: https://www.sciencedirect.com/science/article/pii/S0141635916303038. doi:10.1016/j.precisioneng.2016.10.008

[22] Lim TY, Ratnam MM. Edge detection and measurement of nose radii of cutting tool inserts from scanned 2-D images. Opt Lasers Eng 2012;50(11):1628–1642. URL: https://www.sciencedirect.com/science/article/pii/S0143816612001479. doi:10.1016/j.optlaseng.2012.05.007

[23] Gao W, Asai T, Arai Y. Precision and fast measurement of 3D cutting edge profiles of single point diamond micro-tools. CIRP Ann 2009;58(1):451–454. URL: https://www.sciencedirect.com/science/article/pii/S0007850609000080. doi:10.1016/j.cirp.2009.03.009

[24] Novacam . Novacam's Edge radius measurement. 2020. URL: https://www.novacam.com/applications/edge-measurement/

[25] Introduction – robest documentation. 2018. URL: https://robest.readthedocs.io/en/latest/pages/introduction.html

[26] Rusu RB, Cousins S. 3D is here: Point Cloud Library (PCL). In: 2011 IEEE International Conference on Robotics and Automation. Shanghai, China: IEEE. ISBN 978-1-61284-386-5; 2011, p. 1–4. URL: http://ieeexplore.ieee.org/document/5980567/. doi:10.1109/ICRA.2011.5980567

[27] Bruker A. Optical CMM Coordinate Measuring Machine/System. 2023. URL: https://www.alicona.com/en/products/optical-cmm-machine

[28] Kudryavtsev AV. 3D Reconstruction in Scanning Electron Microscope: from image acquisition to dense point cloud. Ph.D. thesis; Université Bourgogne Franche-Comté; 2017. URL: https://tel.archives-ouvertes.fr/tel-01930234

[29] Kudryavtsev AV, Dembélé S, Piat N. Pollen3D. 2020. URL: https://github.com/avkudr/pollen3d

[30] Beb MY, Bekel A, Dembélé S, Rougeot P, Jouffroy-Bapicot I, Lebas LM, Langloi C, Roiban L, Fellah C, Piat N, Thibaud S, Cuny G, Masenelli-Varlot K, et al. Pollen 3D: An Application of 3D Reconstruction for the Scanning Electron Microscope. In: 2021 The International Symposium on Optomechatronic Technology (ISOT). HAL. 2021, 1–2. URL: https://hal.science/hal-03456526.

[31] Beb MY, Dembélé S, Bekel A, Jouffroy-Bapicot I, Thibaud S, Piat N, Lehmann O, Rauch JY, Rougeot P, Lebas LM, Langloi C, Roiban L, Fellah C, Cuny G, Masenelli-Varlot K,et al. Proposal for a complete 3D surface reconstruction using images from a scanning electron microscope (SEM).. In: Frontiers in Optics + Laser Science 2022 (FIO, LS) (2022). Optica Publishing Group. 2022, JW5A.69. URL: https://opg.optica.org/abstract.cfm?uri=FiO-2022-JW5A.69.

[32] BIMU's SA. BIMU's Catalog. 2019. URL: https://www.bimu.ch/

[33] Bradski G. The OpenCV Library. GitHub 2020;URL: https://github.com/opencv/opencv

[34] Johnson SG. The NLopt nonlinear-optimization package. 2019. URL: http://ab-initio.mit.edu/nlopt/

[35] Kratochvil BE, Dong LX, Zhang L, Nelson BJ. Image-based 3D reconstruction using helical nanobelts for localized rotations. J Microsc 2010;237(2):122–135. URL: https://onlinelibrary.wiley.com/doi/abs/10.1111/j.1365-2818.2009.03313.x. doi:https://doi.org/10.1111/j.1365-2818.2009.03313.x; _eprint: https://onlinelibrary.wiley.com/doi/pdf/10.1111/j.1365-2818.2009.03313.x

[36] Jähnisch M, Fatikow S. 3-D vision feedback for nanohandling monitoring in a scanning electron microscope. Int J Optomechatronics 2007;1(1):4–26. URL: https://doi.org/10.1080/15599610701232630. doi:10.1080/15599610701232630; publisher: Taylor & Francis _eprint: https://doi.org/10.1080/15599610701232630

[37] Baghaie A, Tafti AP, Owen HA, D'Souza RM, Yu Z. SD-SEM: sparse-dense correspondence for 3D reconstruction of microscopic samples. Micron 2017;97:41–55. URL: https://www.sciencedirect.com/science/article/pii/S0968432816302268. doi:10.1016/j.micron.2017.03.009

[38] Kudryavtsev AV, Guelpa V, Rougeot P, Lehmann O, Dembélé S, Sturm P, et al. Autocalibration method for scanning electron microscope using affine camera model. Mach Vis Appl 2020;31(7):69. URL: https://doi.org/10.1007/s00138-020-01109-x. doi:10.1007/s00138-020-01109-x

[39] Xie J. Stereomicroscopy: 3D Imaging and the Third Dimension Measurement 2011:8

Table 1
Results obtained from the virtual tool without and with noise.

No. test	Edge Radius without noise [μm]	Error (%)	Edge Radius With noise [μm]	Error (%)
1	8.07	0.25	8.02	0.37
2	7.95	1.24	7.96	1.12
3	8.03	0.25	8.13	0.99
4	8.03	0.25	8.17	1.49
5	8.08	0.37	8.2	1.86
6	8.04	0.12	8.12	0.87
7	8.11	0.75	8.15	1.24
8	8.08	0.37	8.23	2.24
9	8.09	0.50	8.06	0.12
10	8.04	0.12	8.11	0.75
Average	**8.052**	**0.42**	**8.115**	**1.11**
Repeatability	**0.014**	-	**0.026**	-
Uncertainty	**0.045**	-	**0.082**	-

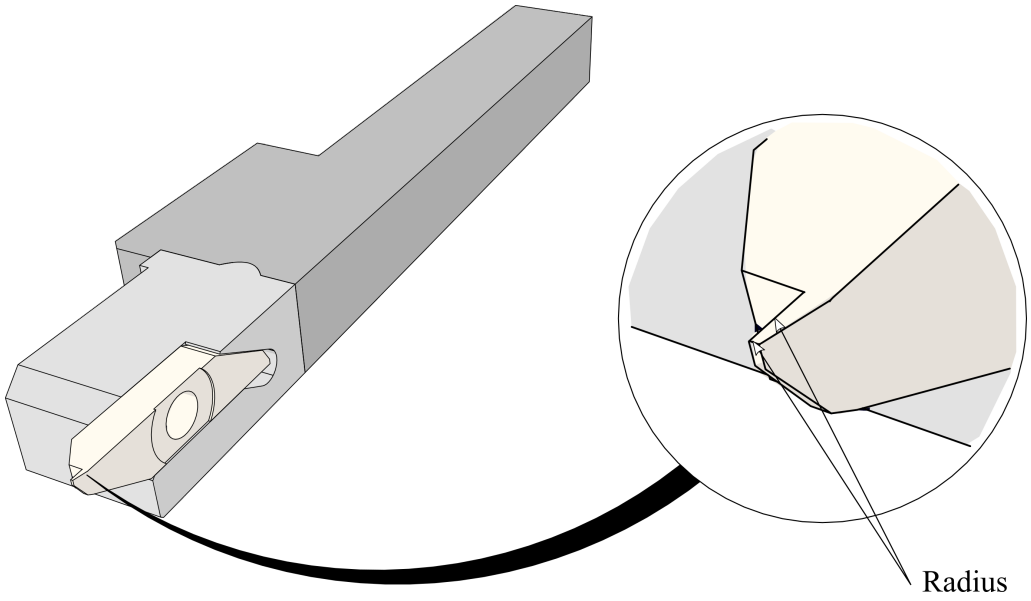

Fig. 1: Microturning tool used to illustrate the method of measurement: inside tool holder (left), zoom on edge (right).

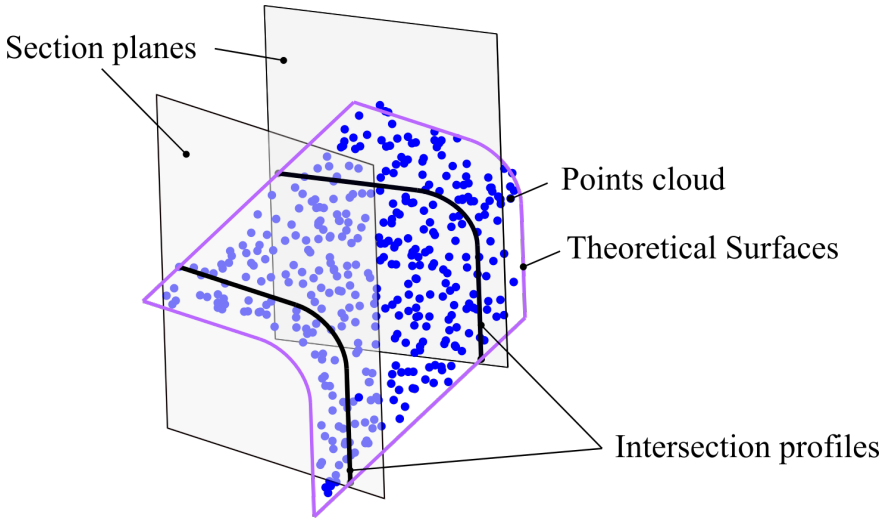

Fig. 2: Geometrical entities when determining the cutting edge radius by conventional procedure. The 2D orientation of the cross-section planes directly affects the determined radius.

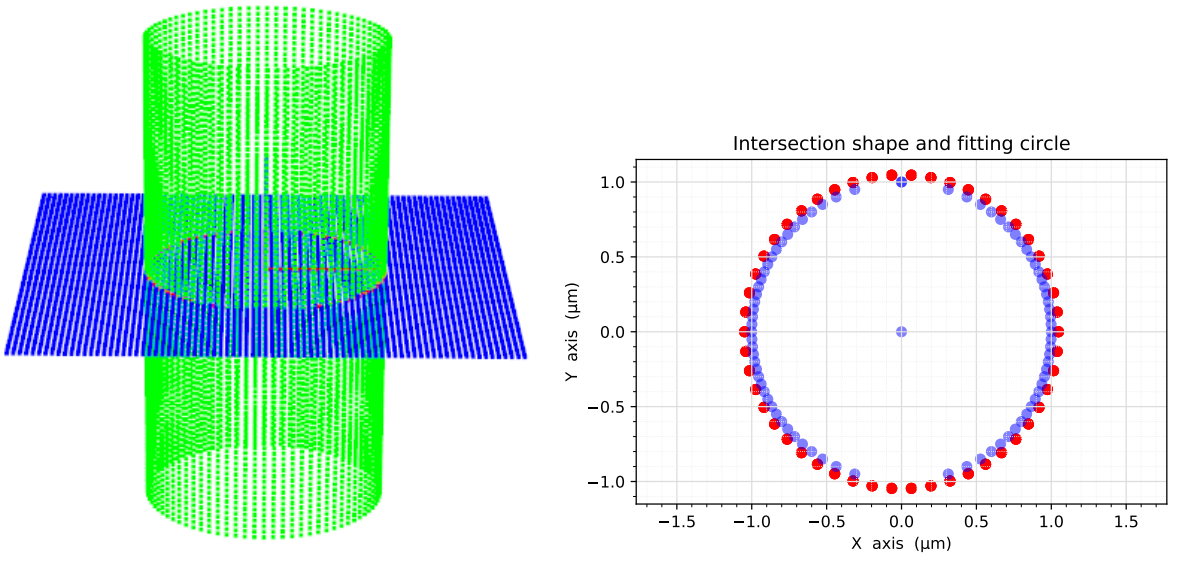

Fig. 3: Intersection between a plane (without inclination) and a cylinder: intersection shape (in blue) and fitted circle (in red, radius: 1.04 µm).

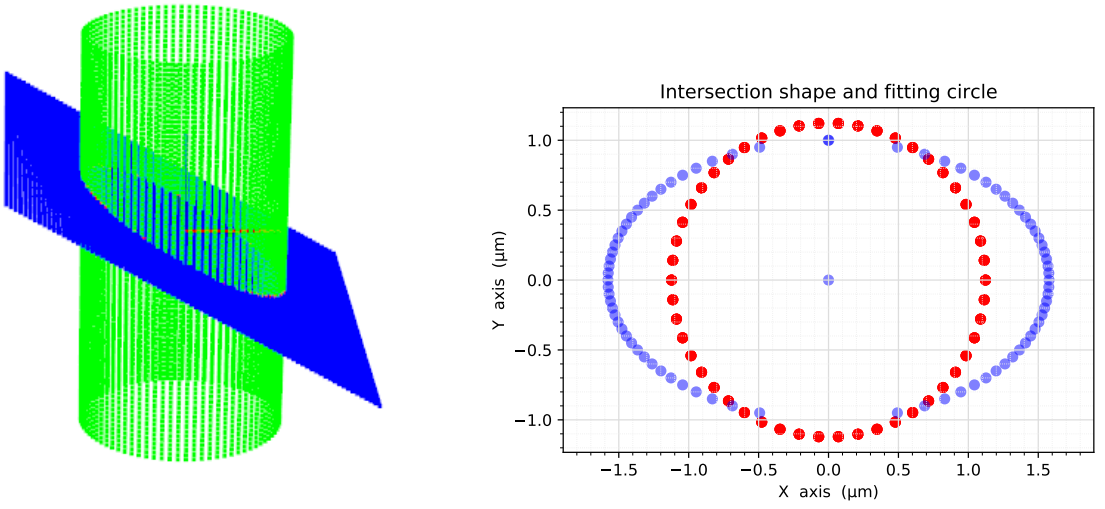

Fig. 4: Intersection between a plane (inclined at 30°) and a cylinder: intersection shape (in blue) and fitted circle (in red, radius: 1.12 µm).

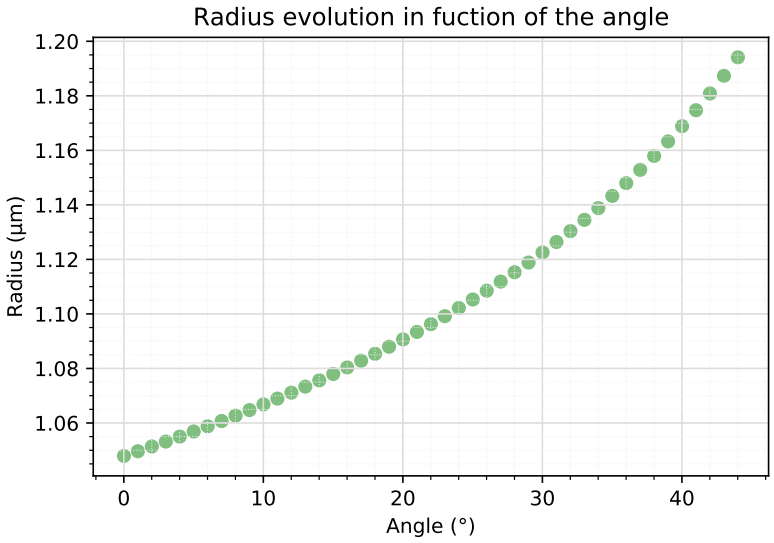

Fig. 5: Influence of the perpendicularity between the plane and the cylinder: radius of the fitted circles according to the variation in the angle of inclination of the plane between 0° and 45.

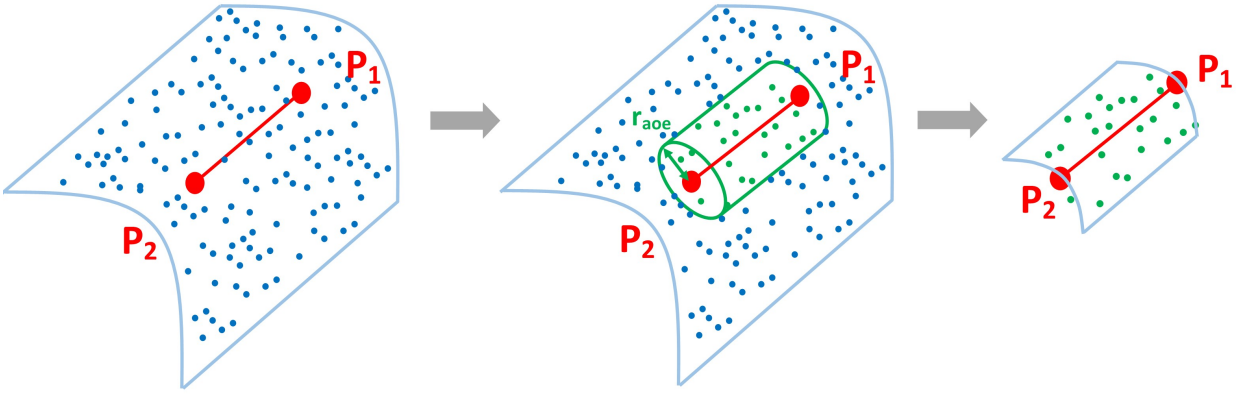

Fig. 6: From key points to global ROIs.

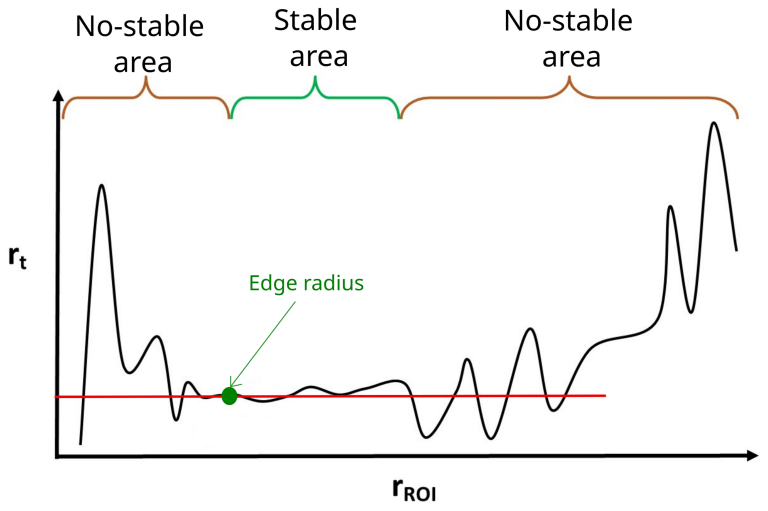

Fig. 7: Theoretical curve of the edge radius vs. the ROI radius.

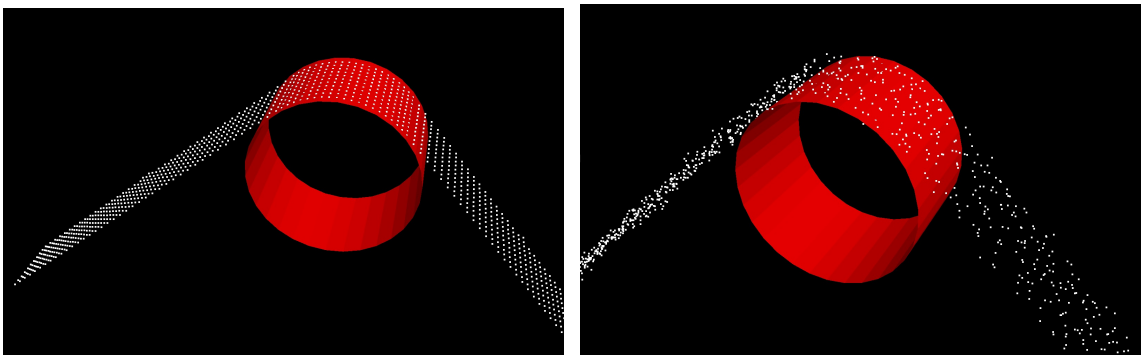

(a) (b)

Fig. 8: Virtual tool edge point cloud: (a) without noise and (b) with noise, with $3\sigma = 1$ µm variance.

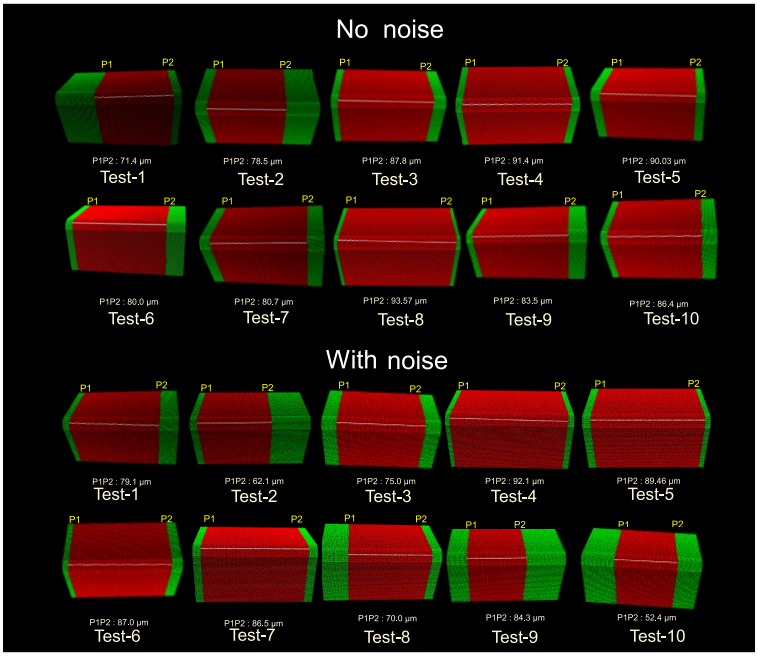

Fig. 9: Different $P1$ and $P2$ were selected in the tests carried out with the simulated point cloud without noise.

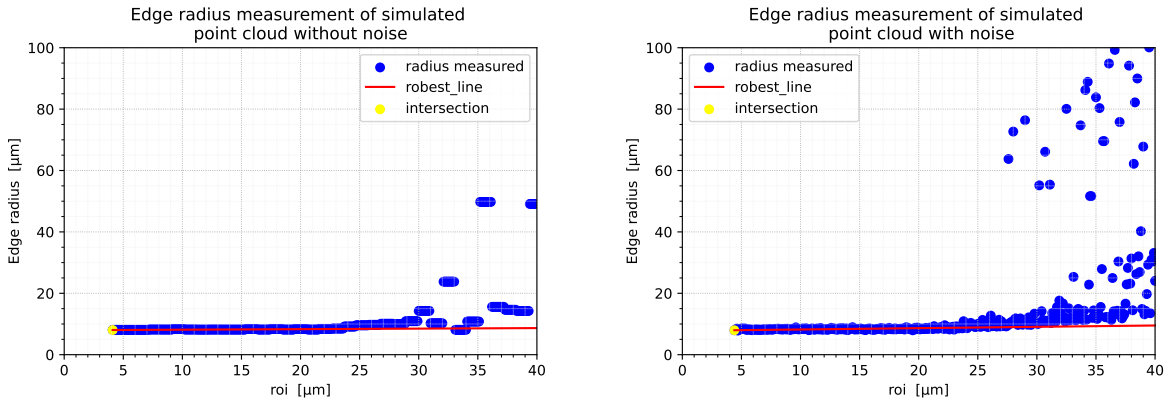

(a) (b)

Fig. 10: Radius measurement for a virtual tool. (a) Measurement of the virtual tool edge without noise. The measured radius was 8.03 µm. (b) Radius measurement of the virtual edge with the point cloud corrupted with normal noise. The measured radius was 7.96 µm.

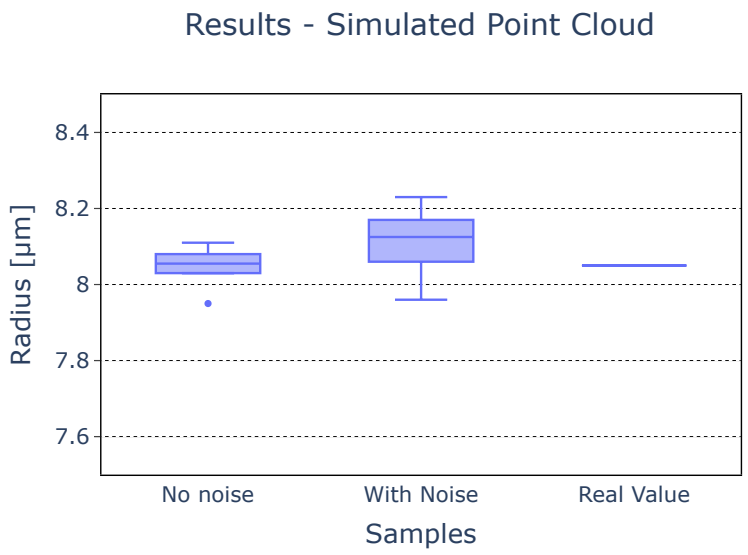

Fig. 11: Results obtained with the virtual tool without noise and the virtual tool with noise compared to that with ground truths.

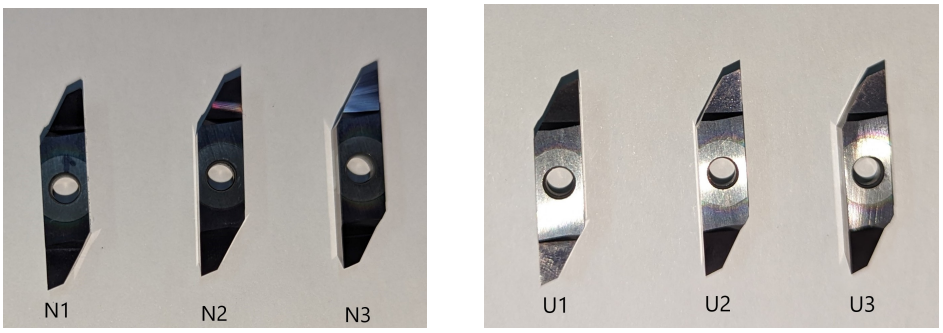

(a) Unused tools (b) Used tools

Fig. 12: An optical image of the six experimental tools (micro-precision Swiss turning tool 050RK18BI90 from BIMU SA [32]).

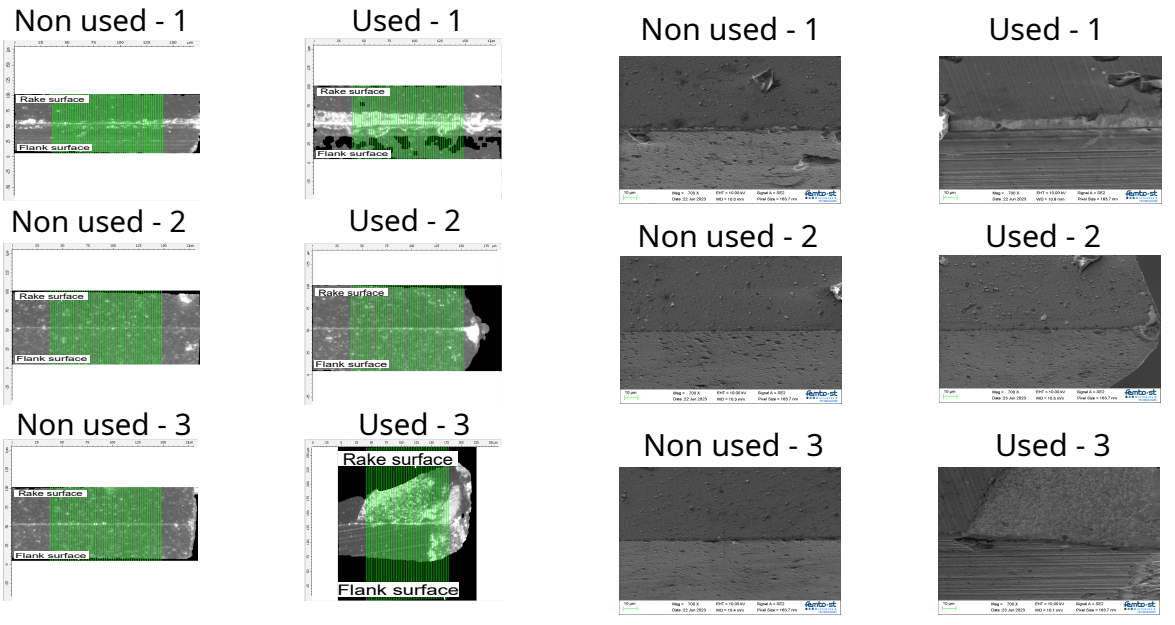

(a) Photo microscopy images (b) SEM images

Fig. 13: Photon microscopy and SEM images. The smoothing process of the edge due to cutting is visible on the used tool images.

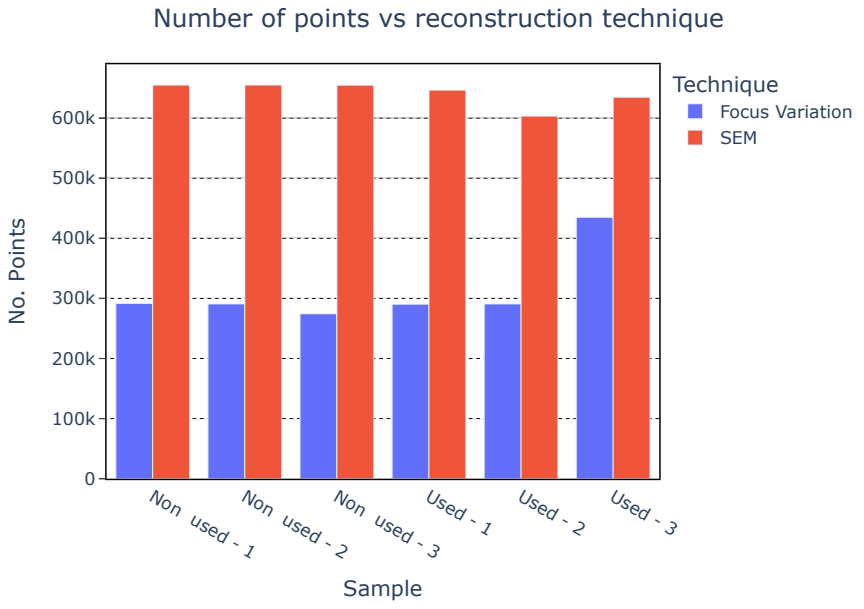

Fig. 14: Comparison between the number of points obtained in the 3D reconstruction of each sample using the two different techniques.

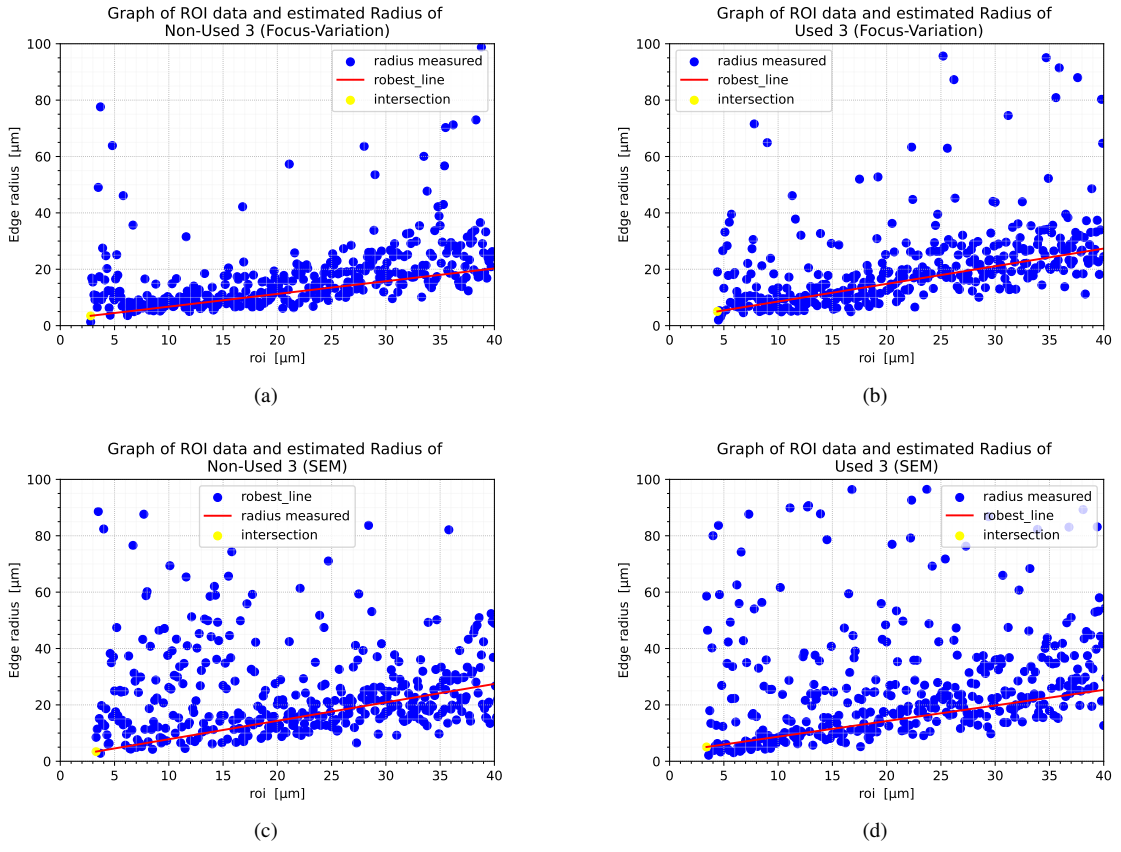

Fig. 15: Examples Radius measurement: (a) Non used tool-3 with robust cylinder fitting (focus variation). The measured radius is 3.48 µm. (b) Used-3 tool with robust cylinder fitting (focus variation). The measured radius is 5.04 µm. (c) Non used tool-3 with robust cylinder fitting (multiview stereo). The measured radius is 3.43 µm. (d) Used-3 tool with robust cylinder fitting (multiview stereo). The measured radius is 5.06 µm.

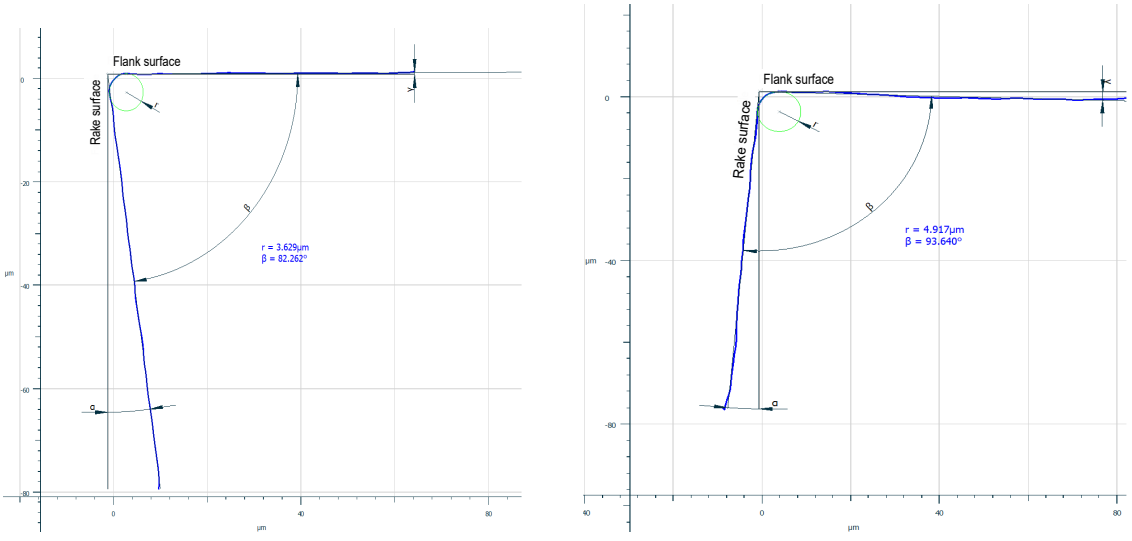

(a) Non Used-3 tool (b) Used-3 tool

Fig. 16: Results with circle fitting (Alicona software) using a point cloud obtained from focus-variation/photon microscopy.

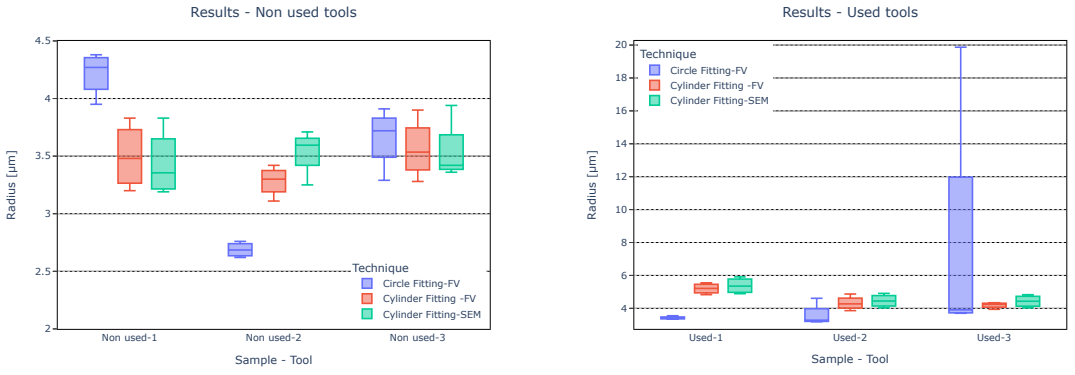

(a) (b)

Fig. 17: Results: (a) Unused tools - using three scenarios (circle fitting with focus-variation/photon microscopy, cylinder fitting with focus-variation/photon microscopy, cylinder fitting with multi-view stereo/SEM). (b) Used tools - using the same three scenarios.